Supplementary materials for Multimode Trapped Interferometer with Non-interacting Bose-Einstein Condensates

Leonardo Masi,[1,2] Tommaso Petrucciani,[2,3] Alessia Burchianti,[1,2] Chiara Fort,[1,2,3] Massimo Inguscio,[1,2,4] Lorenzo Marconi,[1] Giovanni Modugno,[1,2,3] Niccolò Preti,[3] Dimitrios Trypogeorgos,[5] Marco Fattori,[1,2,3] and Francesco Minardi[1,2,6]

[1] *CNR-INO, Istituto Nazionale di Ottica, 50019 Sesto Fiorentino, Italy*
[2] *European Laboratory for Nonlinear Spectroscopy - LENS, 50019 Sesto Fiorentino, Italy*
[3] *Dipartimento di Fisica e Astronomia, Università di Firenze, 50019 Sesto Fiorentino, Italy*
[4] *Dipartimento di Ingegneria, Campus Bio-medico Università di Roma, 00128 Roma, Italy*
[5] *CNR Nanotec, Institute of Nanotechnology, 73100 Lecce, Italy*
[6] *Dipartimento di Fisica e Astronomia, Università di Bologna, 40127 Bologna, Italy*

(Dated: November 2, 2021)

I. KAPTIZA-DIRAC DIFFRACTION WITH A BEAT-NOTE SUPER LATTICE

The beat-note super lattice (BNSL) is generated by overlapping two standing waves at slightly different wavelengths: the potential $V(x) = V_1 \cos^2(k_1 x) + V_2 \cos^2(k_2 x)$ generates momentum components at integer multiples of $2\hbar k_1$, $2\hbar k_2$ and $2\hbar(k_1 - k_2) \ll 2\hbar k_1, 2\hbar k_2$, via Bragg transitions [1].

Since we are concerned only with the low momentum components, we can assume that these are generated by the effective periodic potential of Eq. (5) in the main text. As described in [1], in the perturbative regime, i.e. $V_{1,2} \ll \hbar^2(k_1 + k_2)^2/8M$, the peak-to-peak depth of the effective sinusoidal potential is given by the approximate expression:

$$V_{e0} = V_1 V_2 \frac{M}{\hbar^2(k_1 + k_2)^2}.$$

When the depths V_1, V_2 becomes larger, the potential still diffracts wavepackets at integer multiples of the effective momentum $\hbar k = 2\hbar(k_1 - k_2)$, but the perturbative expression above looses validity. In order to clarify this aspect, here we investigate numerically the depth of the effective potential comparing the momentum distributions obtained after a KD pulse with the BNSL and with the effective lattice of a depth given by the above perturbative expression (see Fig. 1 a,b,c). Clearly the approximation of the BNSL with the perturbative effective potential gets worse as we increase the BNSL amplitude.

To identify the range of validity of the perturbative expression, for each value of the BNSL depth we calculate $\psi_{\mathrm{BNSL}}(k)$, the wavefunction in momentum space at the end of the first KD pulse ($\Delta t = 80\mu$s). We also calculate $\psi_{eff}(k)$, the wavefunction for the same KD pulse when the BNSL is replaced by the effective potential. We identify as "optimal", the depth V_{e0}^{opt} of the effective potential such that the fidelity $|\langle\psi_{eff}|\psi_{\mathrm{BNSL}}\rangle|^2$ is maximum. In Fig. (1c) we report the optimal depth of the effective potential as a function of the BNSL depth, assuming $V_1 = V_2$, together with the corresponding fidelity. Comparing the optimal depth with the perturbative expression and we find that the two curves start to deviate at $V_1 \simeq 50E_R$ and that the fidelity drops below 0.9 for $V_1 > 37E_R$. In the reported measurements the BNSL depth was set to $V_1 = V_2 \simeq 90E_R$, i.e. in a region where the perturbative expression is no longer valid. In order to confirm that the long wavelength approximation is still valid, we investigate numerically the population of the diffracted orders as a function of the length of the pulse Δt. In Fig (2) we report the population of the first three diffracted orders and we compare them with the square modulus of the Bessel function $|J_n(V_{e0}\Delta t/2\hbar)|^2$ with $n = 0, 1, 2$. We observe a very good agreement, except for residual little deviations that are mainly due to the fact that the KD pulses with a BNSL diffract atoms also at the large momentum components associated with the two fundamental optical lattices, i.e. at multiples of $2\hbar k_1$ and $2\hbar k_2$.

As explained in the main text, the population of these components can not be exploited for the purpose of the KD interferometer, and it grows as the depth of BNSL increases. In Fig. (3) we show examples of the momentum distribution after a single KD pulse of the BNSL for increasing values of $V_1 = V_2$, together with an estimation of the fraction of atoms diffracted at large momentum components N_{lost} as function of V_1. To evaluate the latter, we consider as "lost" the atoms with momentum $|p| > 4\hbar k$, since this is the maximum observable diffracted order according to numerical calculation.
For our values of KD lattice depths $V_1 = V_2 = 90E_R$, the fraction of lost atoms is of the order of 20%.

II. ANHARMONICITY

Along the direction of the KD lattice the confinement is provided by a laser beam, hence it can be considered harmonic around its minimum only for displacements much smaller than the beam size. As we strengthen the force applied by the magnetic field gradient, the induced displacement of the potential minimum increases.

The most obvious effect of the anharmonic trapping potential is that the oscillation period gets to depend on the energy, thus the spatial recombination after the half (or full) oscillation is imperfect, causing a decrease

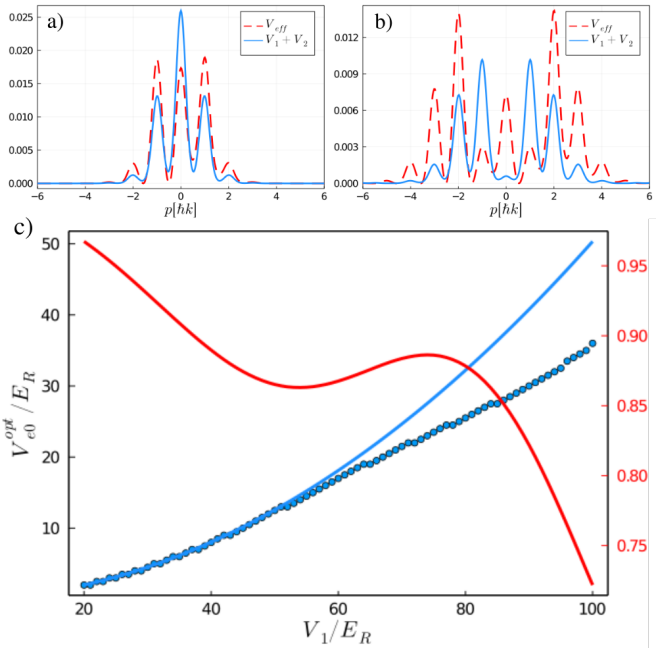

FIG. 1. In the upper panel we compare the momentum distribution after a single KD pulse of the BNSL and of the effective potential with a depth $V_{e0} = V_1V_2M/\hbar^2(k1+k2)^2$ for two different values of $V_1 = V_2$: (a) 80 E_R, (b) 120 E_R. In (c) we report the numerically calculated "optimal" depths (blue points) compared with the perturbative depth (blue line), with the corresponding fidelity (red line, right axis).

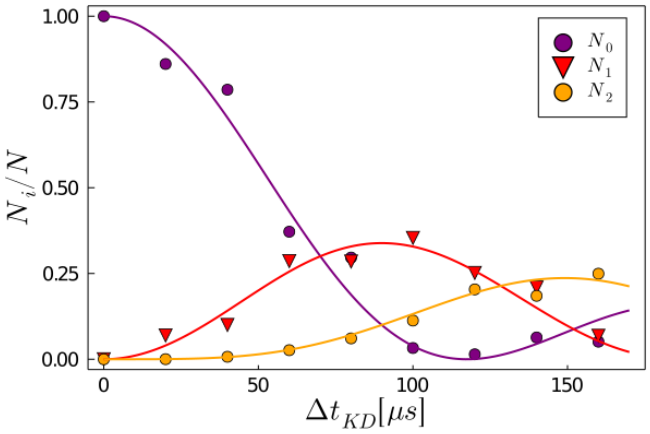

FIG. 2. Numerical atomic fractional populations in the first three momentum components as a function of the length of the pulse for the BNSL with $V_1 = V_2 = 90E_R$ used in the experiment. The solid lines represent the theoretical prediction represented by $|J_n(V_{e0}\Delta t/2\hbar)|^2$, with $V_{e0} = 30E_R$.

of the inteference signal. In addition, the anharmonicity changes substantially the momentum distribution obtained at the interferometer output, as observed in numerical simulations where the trapping harmonic potential is deformed by a quartic anharmonic term [2]. As

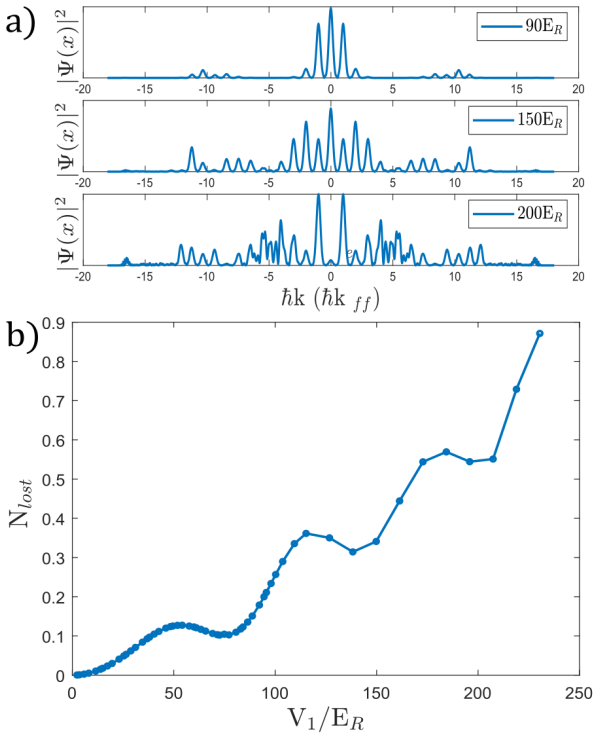

FIG. 3. (a) Momentum distribution after a single KD pulse of the BNSL for different values of $V_1 = V_2$, i.e. 90 E_R (used in the experiment), 150 E_R, and 200 E_R. Both small and large momentum components are displayed, in order to show how the diffraction pattern changes as function of V_1. (b) Fraction of atoms N_{lost} diffracted at momenta larger than the fourth-order component, as a function of V_1.

discussed in the main text, in presence of the harmonic potential the interferometric phase depends only on the position of the relative position of the trap minimum and the KD lattice, because the phase acquired by each wavepacket during half oscillation is zero. This is no longer the case for an anharmonic potential, where the phase acquired by each wavepacket during half oscillation is not zero and is not the same for all wavepackets.

Similarly to [2], we have run numerical simulations to compare the outcome of the interferometer in a harmonic potential and in a Gaussian potential, approximately corresponding to the intensity profile of the laser beam, $V(x) = -V_g \exp(-2x^2/w^2)$ where $w = 100\,\mu$m and the potential depth V_g is adjusted to match the measured frequency of the small-amplitude oscillations.

First, we calculate the overlap between the $0-$th and the $n-$th diffraction orders after half oscillation, i.e. after half-period of the small amplitude oscillations. Fig. 4 clearly shows that, for the above Gaussian potential, the overlap drops for $|n| \geq 3$. Conversely, the overlap is nearly perfect when the atoms populate only $|n| < 2$ diffraction orders, like in our experiment, and it is unity at all orders for the harmonic potential, as expected.

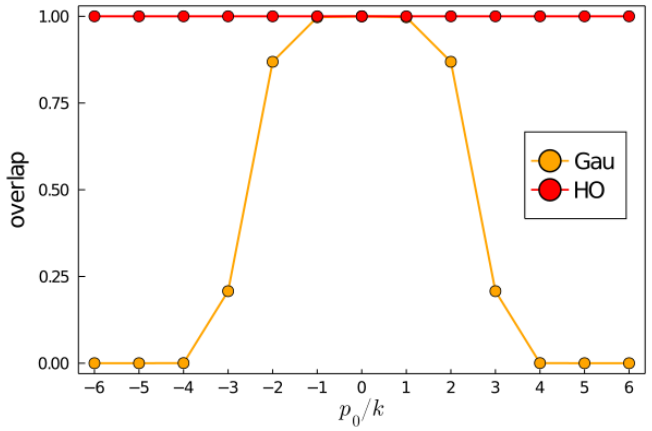

FIG. 4. Overlap $|\langle\psi_0(T/2)|\psi_n(T/2)\rangle|$ of the wavepackets with initial momentum $p_0 = 0$ and $p_0 = n\hbar k$, at time $t = T/2$, i.e. after half period of small-amplitude oscillations: we compare the case of the harmonic oscillator with the Gaussian potential.

We extract the phase shift by fitting the numerically calculated momentum distributions with a sum of 5 Gaussian peaks:

$$f(k) = \sum_{n=-2}^{2} p_0\, J_n^2(p_1)\, \exp[-(k-n)^2/2p_2^2]$$

with p_i, $i = 0, 1, 2$ being free fit parameters. In Fig.(5) we compare the phase shifts ϕ_f obtained from fit, actually $\sin\phi_f = p_1/2\beta$, for the case of the harmonic potential and of the above Gaussian potential. Clearly the deviation is small for the values of external forces and the KD pulse area used in the experiment (solid lines). We notice that the external forces, quantified with the current of the magnetic field gradient as in the main text, here correspond to a maximum displacement of $\sim 2\mu$m much smaller than the beam waist. On the other hand, when the KD pulse area is doubled $\beta = 2.82$, more diffraction orders are populated and the deviation of the Gaussian potential becomes much more visible (orange dashed line). Finally we notice that the slope around zero is $\simeq 1.2$ rad/A for all curves, consistent with the measured value (1.18 ± 0.09) rad/A.

In conclusion, while the anharmonicity of the potential changes the interferometric phase and thus the momentum distribution at the interferometer output, the numerical simulations show that, quantitatively, this effect is nearly negligible for the weak external forces and the KD pulse area of our experiment.

[1] L. Masi, T. Petrucciani, G. Ferioli, G. Semeghini, G. Modugno, M. Inguscio, and M. Fattori, Spatial Bloch Oscillations of a Quantum Gas in a "Beat-Note" Superlattice, Phys. Rev. Lett. **127**, 020601 (2021).

[2] T.-C. He, P.-B. Niu, and J. Li, Measurement of gravitational acceleration by cold atom multimode interference in the anharmonic potential, Annals of Physics **419**, 168227 (2020).

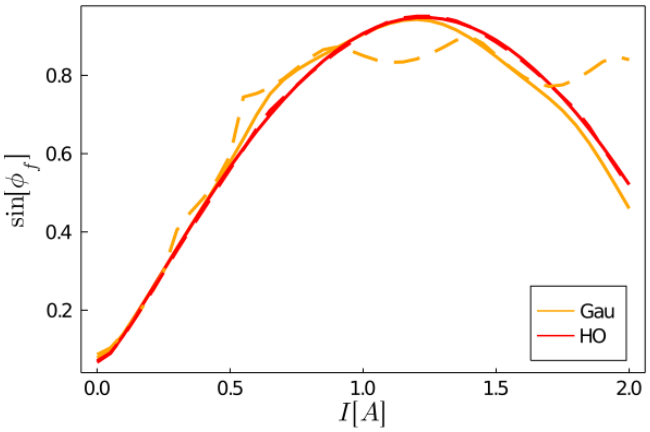

FIG. 5. Phase shifts obtained from fitting the numerically calculated momentum distributions, for the Gaussian and the harmonic potential with the same small-oscillations frequencies: solid lines refer to $\beta = 1.41$, close to experimental value, dashed lines to $\beta = 2.82$.